Journal of Electroanalytical Chemistry 819 (2018) 260–268

Contents lists available at ScienceDirect

Journal of Electroanalytical Chemistry

journal homepage: www.elsevier.com/locate/jelechem

Measurement of competition between oxygen evolution and chlorine evolution using rotating ring-disk electrode voltammetry

J.G. Vos, M.T.M. Koper*

Leiden Institute of Chemistry, Leiden University, PO Box 9502, 2300 RA Leiden, The Netherlands

ARTICLE INFO

Keywords:
Chlorine evolution
Oxygen evolution
Electrocatalysis
Selectivity
Iridium oxide
Rotating ring-disk electrode

ABSTRACT

Selectivity between chlorine evolution and oxygen evolution in aqueous media is a phenomenon of central importance in the chlor-alkali process, water treatment, and saline water splitting, which is an emerging technology for sustainable energy conversion. An apparent scaling between oxygen vs. chlorine evolution has been established, making it challenging to carry the two reactions out individually with 100% faradaic efficiency. To aid selectivity determination, we developed a new method to quickly measure chlorine evolution rates using a conventional RRDE setup. We showed that a Pt ring fixed at 0.95 V vs. RHE in pH 0.88 can selectively reduce the Cl_2 formed on the disk and this allows precise and flexible data acquisition. Using this method, we demonstrate that oxygen evolution and chlorine evolution on a glassy carbon supported IrO_x catalyst proceed independently, and that the selectivity towards chlorine evolution (ε_{CER}) rapidly approaches 100% as [Cl^-] increases from 0 to 100 mM. Our results suggest that on IrO_x, oxygen evolution is not suppressed or influenced by the presence of Cl^- or by the chlorine evolution reaction taking place simultaneously on the surface.

1. Introduction

The electrochemical oxidation of chloride ions is a reaction of great importance to the chemical industry. The electrolysis of brine for the joint generation of Cl_2 and concentrated NaOH, known as the chlor-alkali process, is the most straightforward example [1–3]. This process underpins approximately 50% of the global chemical industry [4], and consumed approximately 334 PJ of electrical energy in the U.S. in 2006 [5]. Another chloride-affected process, which is expected to play a major role in the future energy infrastructure [6–9], is the (photo) electrochemical splitting of water. The latter relies on the endergonic conversion of H_2O into H_2 and O_2, and is typically studied in electrolytes which are [Cl^-]-free. From an industrial perspective however, it would be a great advantage to perform selective electrolysis of saline water, not just for water splitting but also for metal plating, for which OER is usually the desired counter reaction [10,11]. Without a selective anode, there is a risk of forming large amounts of toxic and corrosive Cl_2 gas as byproduct. Lastly, the oxidation of chloride into strongly oxidizing 'active chlorine' may be used to eliminate pollutants in electrochemical wastewater treatment [12,13], but its formation has to be tightly controlled or is sometimes unwanted [14,15].

In brine solutions, the selectivity between the oxygen evolution reaction (OER) and chlorine evolution reaction (CER) is of central importance. In the chlor-alkali process, the OER is a parasitic side reaction that degrades process efficiency and electrode stability [2], whereas it is the desired reaction in saline water electrolysis for hydrogen production. Virtually all known OER catalysts also catalyze formation of chlorine [16–18], indicating that the OER and CER are intimately coupled. This interdependence makes it challenging to carry them out individually with 100% faradaic efficiency.

Both OER and CER have been the subject of intense study over the past five decades, with significant improvements in catalyst performance for both reactions [1]. Today, TiO_2-supported mixtures of RuO_2, IrO_2 and varying metal dopants (Dimensionally Stable Anodes) represent the state of the art materials for industrial water splitting and the chlor-alkali process. Previous work on the CER in aqueous media has generally been done in acidic solutions with very high Cl^- concentrations, often in the range of 3–5 M [19–25]. CER activity and Tafel slopes in such studies were derived from raw electrode current densities, with the assumption that all observed current could be ascribed to CER and that OER plays only a negligible role. Although this assumption is reasonable for high Cl^- concentrations, a complete picture of the competition between OER and CER behavior in chloride-containing media cannot be drawn in this way. If we want to develop anodes selective for OER from (acidic) brine solutions, we will need to understand this competition in more detail, and a reliable and easy method for the determination of the selectivity between OER and CER would be of great interest.

* Corresponding author.
E-mail address: m.koper@chem.leidenuniv.nl (M.T.M. Koper).

http://dx.doi.org/10.1016/j.jelechem.2017.10.058
Received 28 July 2017; Received in revised form 23 October 2017; Accepted 25 October 2017
Available online 28 October 2017

An analytical method to measure Cl_2 and O_2 evolution separately, irrespective of chloride concentration, is Differential Electrochemical Mass Spectrometry (DEMS) [26–30], which directly probes O_2 vs. Cl_2 formation near the electrode surface and can provide highly accurate and quantitative results online [31–33]. However, DEMS suffers from some inflexibility due to specific cell and electrode requirements, and relatively slow response times. Alternatively, a common method of selectivity determination is long-term bulk electrolysis, followed by titration of the working solution using diethyl-phenylenediamine salts (DPD) or iodometry, to determine the amount of Cl_2 formed [33–36]. Such methods, although accurate, are not suitable for generation of extended data sets and do not offer the on-line selectivity determination that DEMS does.

In this paper, we develop and study the suitability of a rotating ring-disk electrode (RRDE) setup for measuring OER vs. CER selectivity in acidic chloride-containing media. The RRDE method has been well established for faradaic efficiency (FE) measurements in benchmarking OER catalysts [37–39], and for the detection of the formation of H_2O_2 during the oxygen reduction reaction (ORR) on model PEM fuel cell cathodes [40–42]. To the best of our knowledge, an RRDE approach for OER vs. CER selectivity measurements has not been previously reported. We used a Pt ring for Cl_2 detection during catalyst operation, as Pt was previously established as an effective CRR catalyst [43]. Other materials (such as Ru or Ir) may also be possible for Cl_2 detection [44], but we have not pursued this in detail. As proof of concept, we explore the CER vs. OER behavior of IrO_x nanoparticles, as this material constitutes a stable and active acidic OER and CER catalyst.

2. Experimental

$KHSO_4$ (EMSURE), KCl (EMSURE), and $HClO_4$ (60%, EMSURE) were purchased from Merck. Na_2IrCl_6 (99.9%, trace metals basis) and NaOH (30% solution, TraceSelect) were purchased from Sigma-Aldrich. All chemicals were used as received. The water used for cleaning glassware and preparing solutions was filtered and deionized using a Merck Millipore Milli-Q system (resistivity 18.2 MΩ cm^{-1}, TOC < 5 p.p.b.). Experiments were done in a home-made two-compartment borosilicate glass cell of 100 mL volume. IrO_x deposition experiments were done in a borosilicate glass vial of approximately 5 mL. Before the first-time use, all glassware was thoroughly made free from organic contaminants by boiling in a 3:1 mixture of concentrated H_2SO_4 and HNO_3. When not in use, all glassware was stored in a 1 g/L solution of $KMnO_4$ in 0.5 M H_2SO_4. Before each experiment, glassware was thoroughly rinsed with water, and then submerged in a dilute solution of H_2SO_4 and H_2O_2 to remove all traces of $KMnO_4$ and MnO_2. The glassware was then rinsed three times with water, followed by triple boiling in Millipore water.

All experiments were carried out at room temperature (~20 °C). Hydrodynamic measurements were performed using an MSR rotator coupled to E6 ChangeDisk RRDE tips in a PEEK shroud (Pine Research Instrumentation). As counter electrode, a Pt mesh separated from the main solution by a glass frit was used. The reference electrode was a HydroFlex® reversible hydrogen electrode (Gaskatel). All potentials in this paper are reported using the RHE scale. Using a Luggin capillary, the RHE reference was aligned to the center of the RRDE tip to minimize electrical cross-talk [45,46]. The liquid phase collection factor of the ring-disk system, N_l, was determined to be 0.245 in at least four separate experiments, where the GC disk was exchanged in between. The value was found using a conventional collection factor experiment on a freshly prepared blank GC electrode with Pt ring, studying the reduction/oxidation of 10 mM $K_3Fe[CN]_6$ in 0.1 M KNO_3.

0.5 M $KHSO_4$ solutions were used for all CER activity experiments. pH values were 0.88 ± 0.05, as measured with a Lab 855 meter equipped with a glass electrode (SI Analytics). pH values were verified by measuring the potential of a calibrated Ag/AgCl reference electrode in the solutions. All working solutions were saturated with either O_2 or Ar (Linde, purity 6.0) before experiments. Mild gas bubbling through the solution was allowed during forced convection experiments, in all other cases gas was used to blanket the solution.

Electrochemistry experiments were controlled with an IviumStat potentiostat (Ivium Technologies). For all experiments, the solution resistance was measured with electrochemical impedance spectroscopy, by observing the absolute impedance in the high frequency domain (100 KHz). Potentials were 85% corrected for these values during measurements. Before a CER activity experiment, the Pt ring was electropolished by cyclic voltammetry (CV) from −0.1 V to 1.7 V at 500 mVs^{-1} for 30 scans at a 1500 RPM rotation rate, after which the individual scans did not change. This step is vital to remove traces of alumina, as well as traces of IrO_x that tend to remain on the ring after being swept outward during IrO_x electroflocculation under rotation [47]. OER and CER experiments were done under hydrodynamic conditions at 1500 RPM by scanning the disk electrode in the range of 1.3–1.55 V at 10 mVs^{-1}. For quantitative analysis, the forward and backward sweeps were averaged to reduce contributions from double layer charging and IrO_x pseudocapacitance. The ring was kept at 0.95 V during CER Faradaic Efficiency measurements, as 0.95 V is in the diffusion-limited regime of Cl_2 reduction but still too positive to lead to oxygen reduction (see Results and discussion). In between experiments, the IrO_x film was kept at 1.3 V. Ring currents were corrected for background currents, and also collection delay, which was approximately 200 ms at 1500 RPM. Before proceeding with OER and CER activity measurements, the IrO_x film was treated by performing 20 scans between 1.3 and 1.55 V, in absence of Cl^-. This was done to ensure stable and reproducible catalyst behavior during experiments.

IrO_x nanoparticles electroflocculated on glassy carbon were used as active OER/CER catalyst. The GC support was prepared to a mirror finish by hand polishing with Al_2O_3 down to 0.05 μm particle size, followed by rinsing and 5 min sonication in acetone and water. IrO_x deposition was done from a suspension of IrO_x nanoparticles, obtained from alkaline hydrolysis of $Na_2Ir[Cl]_6$, as previously published [48–50]. The reader may consult the Supporting information for more details.

For iodometry experiments, amperometry was performed for 60s at 1500 RPM in 16 mL of 0.5 M $KHSO_4$, in the presence of Cl^-, followed by titration of the bulk solution. Under identical conditions, amperometry was performed for 20 s and the Pt ring was used to measure selectivity towards CER. This selectivity was then applied to disk currents of the iodometry experiment to calculate the amount of Cl_2 that must have formed according to the RRDE method. In this way, both methods could be applied to a single experiment. The experiments were done in a glass vial without headspace, of approximately 16 mL volume. The vial was vertically elongated to minimize the contact area of the solution with air, and thus to prevent gaseous Cl_2 from escaping the acidic solution. All solutions were pretreated by briefly evolving chlorine and then purging the solution with Ar. Immediately after finishing an experiment, a large (~100 ×) excess of NaI was rapidly added to the solution to trap all Cl_2 as I_3^- and to minimize the equilibrium concentration of volatile I_2. The vial was then closed air-tight and the solution was allowed to equilibrate for approximately 1 min. Iodometry was performed directly after. Reported values were the average of four titrations. For the sake of verification, RRDE experiments in the iodometry vial were compared to those in a standard glass RRDE cell of 100 mL volume. Although the absolute measured currents of the iodometry vial were slightly lower than the RRDE cell, the ratio i_R/i_D (the 'apparent chlorine collection factor', N_{Cl_2}) was found to be exactly the same, indicating proper transport of Cl_2 from the disk to the ring in the iodometry vial. This justifies the comparison of our RRDE method and iodometry. We attribute the lower CER currents in the small volume iodometric cell to distortion of the hydrodynamic flow field, leading to lowered Cl^- mass transport.

3. Results and discussion

3.1. Aspects of selectivity between OER and CER

There are some important considerations for the apparent selectivity of OER vs. CER, which are also directly relevant to our RRDE method for CER detection. On the RHE scale, the OER and CER in acidic media are given by the following redox reactions with their corresponding standard equilibrium potentials:

$$2H_2O \rightarrow O_2 + 4H^+ + 4\,e^-$$
$$E^0_{O_2/H_2O} = 1.229\ \text{V vs. RHE} \quad (1)$$

$$2\,Cl^- \rightarrow Cl_2 + 2\,e^-$$
$$E^0_{Cl_2/Cl^-} = (1.358 + 0.059\ \text{pH})\ \text{vs. RHE} \quad (2)$$

The CER exchange current density was previously reported being generally 4–7 orders of magnitude higher than OER [51], due to the more facile catalysis of a two-electron process vs. a four-electron process [52]. For pH ≈ 1, assuming an overpotential of 0.25 V for the OER and 0 V for CER, this leads to the situation that in the potential window of 1.42 V < E < 1.48 V, Cl_2 can be evolved exclusively despite thermodynamic preference for OER. With increasing pH, the equilibrium potential of the CER will shift to higher potentials relative to OER, and at high pH the selectivity between the two reactions is expected to be dictated by thermodynamics. A possibly complicating factor is the generation of protons from OER, which can drastically lower the pH near the electrode surface and shift the CER onset to lower values [3,53,54]. This problem is expected to be much less severe near pH ≈ 1, because of the high initial proton concentration.

More importantly, at higher pH, the direct electrochemical formation of hypochlorous acid or hypochlorite becomes thermodynamically more favorable than CER:

$$Cl^- + H_2O \rightarrow HClO + H^+ + 2e^-$$
$$E^0 = (1.482 + 0.030\ \text{pH})\ \text{V vs. RHE} \quad (3)$$

$$Cl^- + H_2O \rightarrow ClO^- + 2H^+ + 2e^-$$
$$E^0 = 1.636\ \text{V vs. RHE} \quad (4)$$

These reactions are expected to compete with CER at pH ≈ 4 and pH ≈ 4.7, respectively. These redox reactions come into play because higher pH favors the disproportionation of Cl_2 into hypochlorous acid and hypochlorite, according to

$$Cl_2(aq) + H_2O \rightarrow HClO(aq) + H^+ + Cl^-$$
$$pK_a = 2.98 \quad (5)$$

$$HClO(aq) \rightarrow H^+ + ClO^-$$
$$pK_a = 7.53 \quad (6)$$

Contrary to CRR, the reduction of ClO^- and HClO are sluggish reactions on Pt, which reach diffusion limited conditions only at overpotentials near $\eta = 1$ V [55,56]. As such, we do not expect it possible to quantify these species by means of the RRDE, since the criterion of reaching diffusion limitations before ORR (which has an onset of approximately 0.95 V on Pt) cannot be reached. The formation of ClO^-/HClO thus has to be kept minimal, and $Cl_2(g)$ is the desired chlorine species for reduction. Summarizing, we expect that the RRDE approach is limited to acidic environments (pH < 2), where the focus is on direct (kinetic) competition of OER vs. CER, and where both products are gases dissolved in the working solution.

3.2. Application of the RRDE to OER vs. CER selectivity measurements

To demonstrate the application of our RRDE method to measure CER, Fig. 1 shows the forward and backward scan average of an IrO_x catalyst in the potential region of 1.3–1.55 V, in acidic media and in presence of 20 mM Cl^-. Fig. S1 in the Supporting information shows a typical characterization CV in the region 0 V–1.4 V. In Fig. 1, the disk current (black line) is measured until 1.55 V, leading to a competition between OER and CER above ca. 1.48 V. The Pt ring (grey line) was fixed at $E_R = 0.95$ V and performs diffusion-limited reduction of Cl_2 (CRR, see next section). The ring potential 0.95 V was chosen well in the diffusion-limited regime of CRR near the edge of ORR onset on Pt in a chloride-free solution. In this way, the ring allows very precise observation of the onset and the rate of the CER.

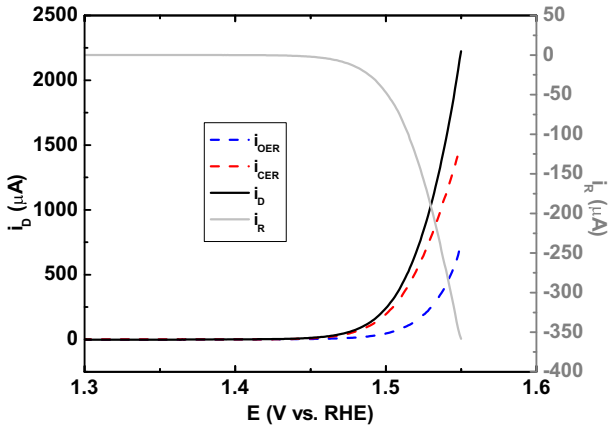

Fig. 1. CV of IrO_x/GC in the OER + CER region in 0.5 M $KHSO_4$ + 20 mM KCl, scan rate 10 mVs^{-1}, rotation rate 1500 RPM. pH = 0.88, solution saturated with Ar. Ring potential was fixed at $E_R = 0.95$ V. The forward and backward scans of the disk were averaged, i_R was corrected for collection delay. i_{OER} and i_{CER} curves were calculated as described in the text. (For interpretation of the references to color in this figure legend, the reader is referred to the web version of this article.)

To minimize capacitive charging contributions on the disk, a relatively slow scan rate of 10 mV/s was used, and values of forward and average scans were averaged. The magnitude of capacitive charging in the potential region of 1.3 V to approximately 1.4 V, where IrO_x experiences the onset of the Ir(IV) to Ir(V) transition, was approximately 10 μA. Such currents were usually < 1% of the OER charge measured. Taking the average of forward and backward scans eliminated most of this possible source of error, noting that our IrO_x showed no significant hysteresis in the 1.3–1.55 V potential range (see Fig. S1).

Since IrO_x is established as a stable acidic OER catalyst within the time frame of our experiments [57], we assume that the measured disk current can be ascribed exclusively to either OER or CER, after minimizing capacitive contributions. From the ring current, we can separate the current contributions of OER and CER on the disk. Since the reaction taking place on the ring (CRR) is simply the reverse of CER, the current contribution originating from CER, i_{CER}, will be

$$i_{CER} = \left|\frac{i_R}{N_l}\right| \quad (7)$$

where i_R is the current measured on the ring, and N_l is the liquid phase collection factor ($N_l = 0.245$). The OER current contribution is simply the current remaining after CER subtraction:

$$i_{OER} = i_D - i_{CER} = i_D - \left|\frac{i_R}{N_l}\right| \quad (8)$$

where i_D is the current measured on the disk. In Fig. 1, i_{OER} and i_{CER} (blue and red dotted lines) were constructed by the above method. The OER onset is near 1.480 V, equivalent to an overpotential $\eta_{OER} \approx 0.25$ V, in good agreement with previous studies [48,58]. As expected, CER shows a much earlier onset of ~1.420 V, equivalent to a negligible overpotential at pH = 0.88.

At this point we must describe a significant caveat, namely, that there is always the risk of forming gas bubbles at high current densities. The problem is mainly related to high OER currents, which may rapidly lead to local supersaturation of poorly soluble O_2 [59–61]. Gas bubbles

may strongly persist on the electrode surface and hinder the transport of products to the ring [54], compromising the quantitative nature of the experiment. This is a universal problem in the use of RRDE for gas forming reactions and makes OER FE experiments at high overpotentials extremely challenging (for example, N_{O_2}, the apparent collection factor for O_2, is often found to be approximately 0.19, much lower than the ideal value) [37,48,62,63]. The solubility of Cl_2 at pH 1 is approximately 10^3 times higher than that of O_2 [64], making high CER currents less troublesome, although extreme CER current densities may additionally lead to formation of Cl_2 bubbles. In our experience, when performing scanning experiments at 10 mVs^{-1} up to 1.55 V, a suitable potential window is limited to peak OER currents of approximately 10 $mA\,cm^{-2}$. A straightforward test for disk-ring transport problems is to perform multiple scans, and to verify whether the ring current decreases over time.

3.3. Effect of chloride adsorption and PtO_x formation on chlorine detection with the Pt ring

To explore the behavior of CRR (and ORR) on the Pt ring in presence of Cl^-, we used the disk to generate a stepwise increasing Cl_2 flux, by fixing the disk potential in the range 1.420 V < E_D < 1.480 V, where only CER is expected to occur at pH = 0.88 (see also Fig. 1). We simultaneously recorded forward linear sweep voltammograms at 1500 RPM on the ring, using a slow scan rate of 5 mVs^{-1} to minimize transient charging current. The steady state disk currents and corresponding ring LSV profiles are shown in Fig. 2. The working solution was saturated with O_2 to accurately monitor the ORR onset as function of [Cl^-] and (locally) [Cl_2]. We assume that the increased concentration of O_2 does not majorly affect CRR kinetics.

In Fig. 2, the ring first traverses a region of superimposed ORR and CRR between 0.2 V < E_R < 0.7 V. When comparing the ORR in chloride-free conditions (grey dashed curve), the ORR onset potential in presence of 100 mM Cl^- is shifted 200 mV negatively, which prohibits the ORR from reaching diffusion limited current before the onset of hydrogen adsorption. Such a suppressing effect was previously observed by Schmidt et al. [65] even at [Cl^-] as low as 100 μM.

Following the ORR + CRR region, a region of constant negative current follows in the range of 0.7 V < E_R < 1.3 V, which we ascribe to CRR under diffusion limited conditions. At potentials higher than

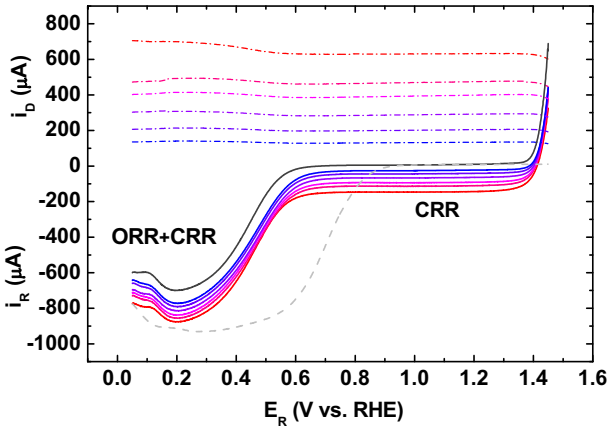

Fig. 2. LSV of the Pt ring electrode, while keeping the IrO_x/GC disk electrode at constant potential in 0.5 M $KHSO_4$ + 100 mM KCl, scan rate 5 mVs^{-1}, rotation rate 1500 RPM. pH = 0.88, solution saturated with O_2. Dotted curves with positive values correspond to disk currents, remaining curves correspond to ring currents. The ring LSV sweeps were taken in the positive-going direction. Disk potentials were chosen in the region of exclusive CER, with values increasing from the blue curve to the red curve, E_D = 1.449 V, 1.456 V, 1.462 V, 1.467 V, 1470 V, and 1.475 V. Black curve shows ring response while disk is not connected. Grey dashed curve shows ring response while disk is not connected, in Cl^--free conditions. (For interpretation of the references to color in this figure legend, the reader is referred to the web version of this article.)

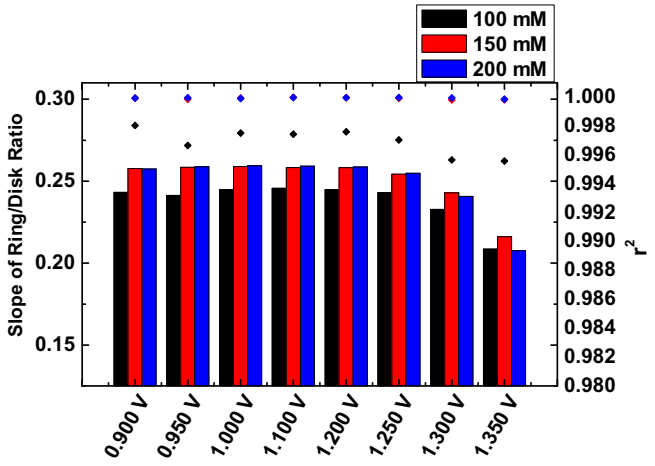

Fig. 3. Apparent chlorine collection factors N_{Cl_2} (equivalent to slopes of ring/disk ratios) plotted as function of potential on the ring electrode, for [Cl^-] = 100 mM (black), 150 mM (red) and 200 mM (blue). Diamonds (correspondingly colored) indicate the determination coefficient r^2 of the found slopes. Data derived from Fig. 2. (For interpretation of the references to color in this figure legend, the reader is referred to the web version of this article.)

1.3 V, the ring approaches E_{Cl_2}/Cl^{-0}, and the onset of CER on the ring can be observed. The experiments shown in Fig. 2 were also performed for [Cl^-] = 150 mM and 200 mM.

It is reasonable to assume that the constant current in Fig. 2 in the region of 0.7 V < E_R < 1.3 V arises from diffusion limited CRR. However, previous studies by Conway et al. [19,66] showed that chloride adsorption causes CER self-retardation on Pt for [Cl^-] ranges near 1 M by affecting the rate-limiting Tafel recombination step. To verify that the ring current response is completely diffusion controlled at E_R = 0.95 V, we propose a simple method: as long as only CER occurs on the disk, a of plot i_R vs. i_D would yield a straight line, with the 'apparent chlorine collection factor' N_{Cl_2} as slope. If N_{Cl_2} approaches the liquid phase collection factor N_l, the ring reaction is indeed diffusion limited, and the measured CRR current is quantitative. Kinetic limitations of CRR on the ring would manifest as N_{Cl_2} < N_l.

Using data from Fig. 2, we plotted the i_R vs. i_D response at various ring potentials (see Fig. S2 in the Supporting information). We generally observed strong linearity between i_R and i_D, with determination coefficients r^2 approaching 1. Furthermore, as shown in Fig. 3, N_{Cl_2} converges to a constant value of ~0.244 for [Cl^-] = 100 mM, and ~0.258 for 150 mM and 200 mM, as E_R is lowered. Only for $E_R \geq$ 1.300 V do we observe ring-disk ratios that significantly differ from these values. At these potentials, E_{Cl_2}/Cl^{-0} is approached (η_{CER} < 100 mV), and CRR kinetics become kinetically limited. For [Cl^-] = 150 mM and 200 mM, the value to which N_{Cl_2} converges is approximately 5% higher than N_l. We ascribe this discrepancy to electrochemical crosstalk [45,46], which we could not eliminate experimentally despite intensive efforts (see also the slight downward slope in disk currents within 1.4–1.45 V, in Fig. 2). Nonetheless, the most important point is that N_{Cl_2} reaches limiting values close or identical to N_l well before the ORR onset potential.

To explore the effect of pH on Cl_2 detection and to corroborate the discussion in Section 3.1 concerning pH-dependent Cl_2 disproportionation into hypochlorous acid, we have probed the apparent chlorine collection factor N_{Cl_2} in pH = 0.90 and pH = 2.91, using a forward linear sweep in a Pt-Pt RRDE setup. Fig. S3 in the Supporting information shows that N_{Cl_2} decreases from 0.242 at pH = 0.90 to 0.214 at pH = 2.91. We ascribe this 12% decrease in collection efficiency to the partial disproportionation of Cl_2 into HClO, a species which is undetectable by Pt at E = 0.95 V. Cl_2 detection is thus no longer quantitative at pH ~ 3, although it could still be used qualitatively, such as for mechanistic studies.

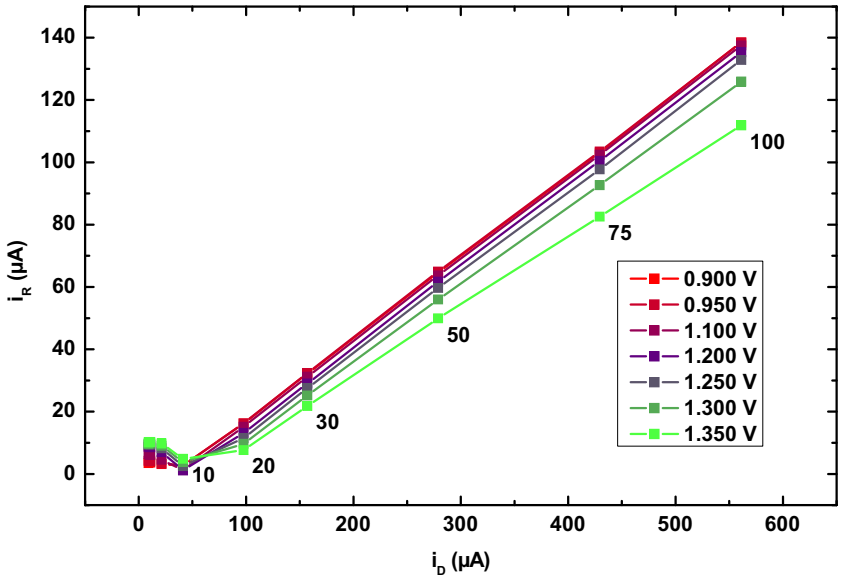

Fig. 4. Behavior of i_R vs. i_D at various ring potentials. IrO_x/GC disk electrode fixed at 1.475 V, in 0.5 M $KHSO_4$ + $[Cl^-]$ increasing from 1 to 100 mM. Numeric labels next to data points show the concentration of chloride, in mM. Labels for $[Cl^-] < 10$ mM are not displayed.

Another factor that needs to be considered for CRR on Pt is the presence of platinum oxide, which is known to be a sluggish CER/CRR catalyst in comparison with Pt. [43,44,66,67] In Fig. 3, where $[Cl^-]$ is always 100 mM or higher, the formation of PtO_x can be assumed absent due to inhibition by Cl^- adsorption [66], but lower $[Cl^-]$ would allow significant growth of oxides. To investigate the presence and effect of PtO_x on CRR, we performed experiments as in Figs. 2 and 3, but instead, we fixed E_D = 1.475 V and studied CRR on the Pt ring as function of $[Cl^-]$ increasing from 1 to 100 mM.

Like Fig. S2, Fig. 4 displays slopes of i_R vs. i_D, together with the corresponding $[Cl^-]$ values. We note that an increase in $[Cl^-]$ will now have a twofold effect: a) it will increase CER current on the disk electrode, leading to higher Cl_2 flux to the ring and thus larger CRR currents, and b) it is expected to progressively inhibit PtO_x growth on the ring, affecting measured ring current profiles. Linearity between i_R vs. i_D is generally observed, except for data for which $[Cl^-] < 10$ mM. The corresponding LSV curves (see Fig. S4 in the Supporting information, inset) suggest significant PtO_x formation is taking place for measurements in the 1–10 mM range when comparing against the black curve taken in Cl^--free conditions. There is clear non-linear behavior of increases in CRR current versus $[Cl^-]$; only for $[Cl^-] > 10$ mM we observe the desired linearity. We explain these results as follows: for very low $[Cl^-]$, detrimental PtO_x formation occurs on the ring in the forward scan within the timescale of our experiments. For $[Cl^-] > 10$ mM, PtO_x growth becomes inhibited and CRR may proceed on an oxide-free surface. For higher chloride concentrations, the i_R vs. i_D slopes show behavior identical to Fig. 3, converging to $N_{Cl_2} \approx 0.247$ as E_R becomes lower.

To summarize our findings regarding the use of a Pt ring for chlorine detection: contrary to ORR, the specific adsorption of chloride at Pt does not seem to have a detrimental effect on CRR, at least not up to $[Cl^-]$ = 200 mM. Somewhat ironically, Cl adsorption actually seems favorable for carrying out CRR as it inhibits the formation of PtO_x, which is detrimental. Furthermore, in case of $[Cl^-] > 10$ mM, ring potentials of 1.250 V already seem adequate to ensure that, at pH 0.88, CRR proceeds diffusion limited. It is however recommended to keep the potential at the lowest possible limit, 0.95 V, to minimize growth and interference of PtO_x at lower chloride concentrations.

3.4. OER vs. CER selectivity as a function of E_D and $[Cl^-]$

Based on the method described in Section 3.2, the faradaic efficiency for CER (ε_{CER}), can be obtained from the relation:

$$\varepsilon_{CER} = \frac{i_{CER}/2}{i_{CER}/2 + i_{OER}/4} \quad (9)$$

Typical results are displayed in Fig. 5. We have plotted the data of three different disk potentials, namely a) 1.48 V, b) 1.52 V and c) 1.55 V. These potentials correspond to regimes where a) CER is present and OER is virtually absent, b) CER is the major reaction but OER takes place with a modest rate, c) both CER and OER take place.

From Fig. 5 we can make several interesting conclusions. The CER activity is approximately linear with $[Cl^-]$ at all potentials, indicating a reaction order of one within the whole potential range. Only at very low $[Cl^-]$ we observe a slope smaller than one, likely due to PtO_x formation on the ring, as discussed in Section 3.3. Furthermore, the OER rates show a constant value for a given E_D as function of $[Cl^-]$, and this trend persists in the entire measured potential range. Thus, the OER does not seem strongly affected by either the presence of Cl^- or the competing CER. Fig. 5 suggests that OER and CER proceed independently within the measured potential range. This implies that OER and CER do not share the same active site on this catalyst, even though a scaling relationship between their activities has been suggested in previous literature [16–18].

Extensive DFT calculations on model RuO_2(110) surfaces have suggested that OER and CER proceed on the same active site, namely, oxygen atoms (O_{ot}) bound to Ru atoms which are coordinatively unsaturated on the pristine model surface [68,69]. Although our results appear to exclude a model of two reactants competing for the same active site, it can be assumed that the amorphous, hydrous IrO_x catalyst in our study is far removed from the Ru single crystalline model surfaces used in the DFT studies, making a direct comparison difficult. Additionally, an independence of OER activity versus $[Cl^-]$ was previously found in DEMS studies on heterometal doped RuO_2 mixtures, indicating that such behavior is not unusual [35,70].

ε_{CER} sharply rises as the chloride concentration increases. Near $[Cl^-]$ = 20 mM, ε_{CER} generally exceeds 80%, and at 40 mM it exceeds 90%. When the chloride concentration increases to 100 mM, ε_{CER} converges to values above 95%. For comparison, Fig. S5 in the Supporting information shows a similar ε_{CER} vs. $[Cl^-]$ plot for commercial RuO_2 (available from Sigma-Aldrich). Interestingly, RuO_2 generally shows a higher selectivity towards CER compared to the IrO_x catalyst, since ε_{CER} converges towards 100% CER more rapidly as $[Cl^-]$ increases.

When the potential increases to 1.55 V, the CER starts becoming diffusion controlled as evidenced by increasingly higher Tafel slopes

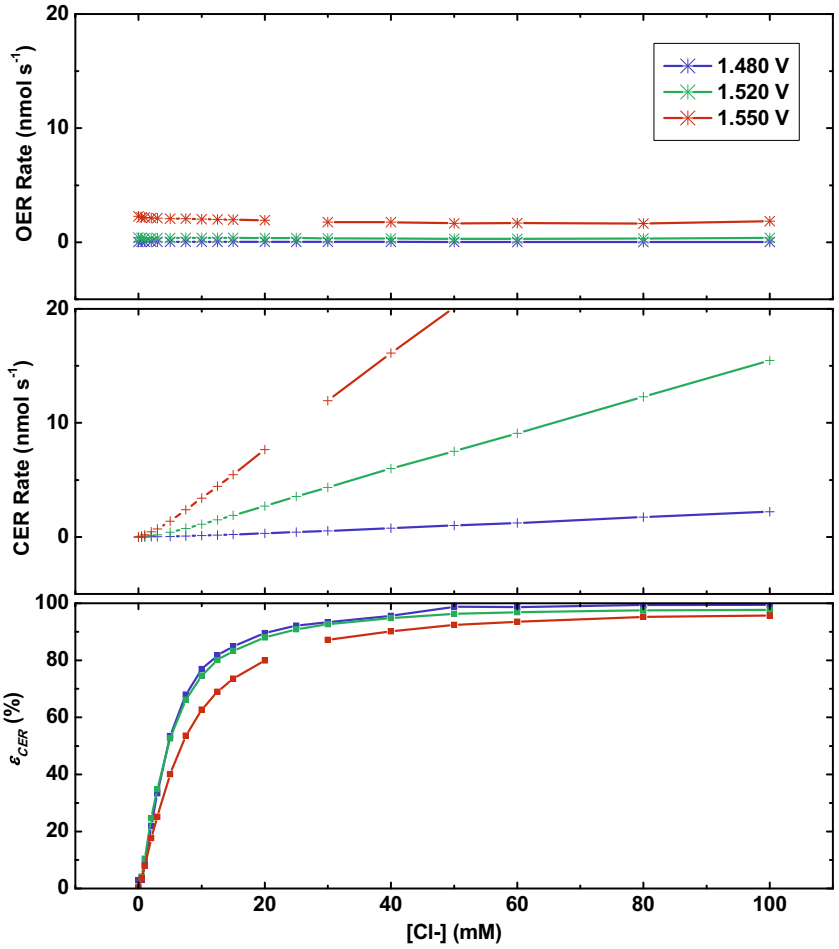

Fig. 5. Plots of OER and CER reaction rates as function of [Cl^-], for three disk potentials: E_D = 1.480 V (blue lines), 1.520 V (green lines), and 1.550 V (red lines). Values were obtained from CVs identical to Fig. 1, while varying [Cl^-]. Rates were obtained by dividing currents by nF, the number of electrons transferred and Faraday's constant. (For interpretation of the references to color in this figure legend, the reader is referred to the web version of this article.)

(not shown), and CER selectivity starts to decrease due to diffusion limitations and increasing contributions of competing OER. There is thus a range of low [Cl^-] where significant (> 10%) OER is present regardless of potential, up to about [Cl^-] = 40 mM. Most importantly, higher potentials of catalyst operation will increasingly favor OER. This trend is very similar to a previous DEMS study on OER vs. CER selectivity on pristine and doped IrO_x nanoparticulate catalysts [71].

We stress that all measurements in this paper were done in presence of 0.5 M HSO_4^-, which is known to absorb on Pt. [72] To investigate the effect of anion adsorption on PtO_x formation and CER detection, we have measured ε_{CER} vs. [Cl^-] in electrolytes of pH ~0.8 composed of 0.5 M $NaHSO_4$ and 0.5 M $NaClO_4$ (Fig. S6 in the Supporting information). A small but clear difference is apparent: although the two electrolytes generally show identical selectivities, ε_{CER} appears to lag behind in low [Cl^-] regimes in presence of non-absorbing ClO_4^-. We ascribe this to a greater degree of PtO_x formation, which hinders Cl_2 detection and distorts the apparent selectivity. As discussed in Section 3.3, the problem resolves itself as [Cl^-] increases.

Owing to the scanning nature of the experiments, we have sampled the complete potential range within 1.3–1.55 V. This allows the construction of 3-dimensional plots showing OER rates and CER rates as a function of E_D and [Cl^-], as shown in Fig. 6. We remark that 'dynamic'

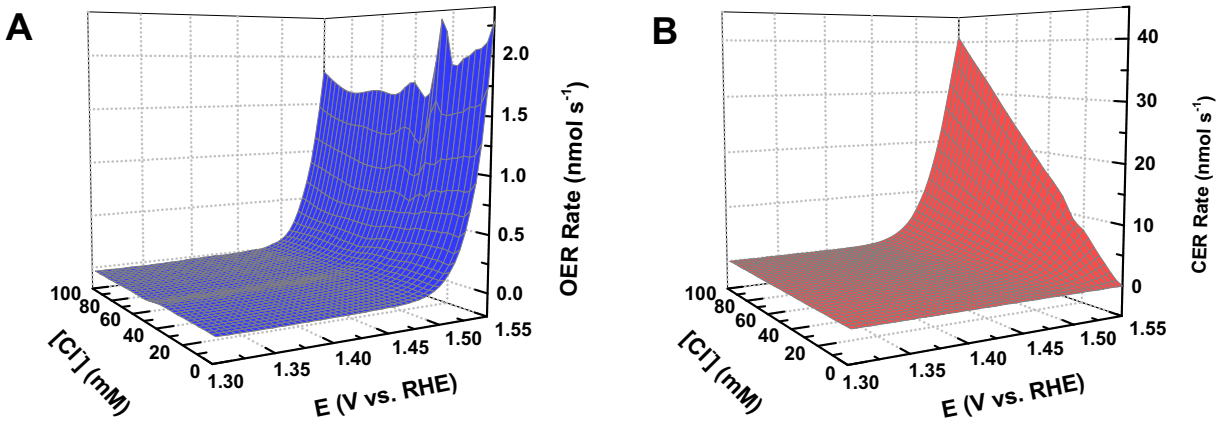

Fig. 6. Plots of A) OER rates and B) CER rates as function of E_D and [Cl^-], constructed from CVs identical to Fig. 1, while varying [Cl^-]. Rates were obtained by dividing currents by nF, the number of electrons transferred and Faraday's constant.

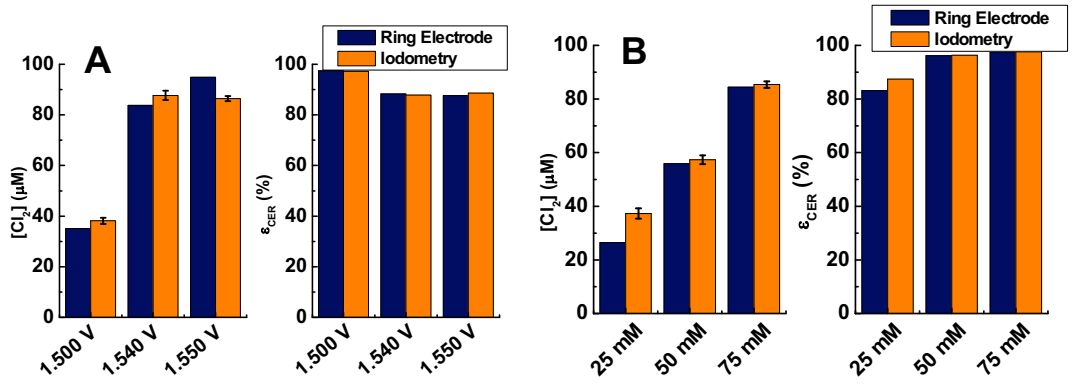

Fig. 7. Cl_2 concentrations and corresponding ε_{CER} as determined by iodometry and the RRDE method, in 0.5 M $KHSO_4$. A: 50 mM KCl, as function of E_D. B: E_D = 1.53 V, as function of [Cl^-]. Error bars show 95% confidence intervals of the titration.

potential methods such as cyclic voltammetry may lead to different catalyst behavior than steady state measurements, especially concerning gas forming reactions [73,74]. In this paper, we have only included cyclic voltammetry to serve as a proof of principle for the RRDE method. Lastly, we stress that plots like Figs. 5 and 6 are only valid for stable catalysts. Side reactions and transient dissolution of the catalyst will distort the results. Caution is advised with the assumption that all remaining current is related to OER.

Finally, to confirm that the RRDE method yields trustworthy results, we employed iodometry to compare values of CER faradaic efficiency as determined by iodometric titration versus those determined by the RRDE method. Values of [Cl_2] were obtained versus E_D and [Cl^-], and agree very well with each other between the two techniques (see Fig. 7). Values of ε_{CER} versus E_D and [Cl^-] correspond to those in Fig. 5, but are approximately 3% lower. As described in the experimental section, we ascribe this difference to a slight hindrance of Cl^- mass transport in the iodometry setup.

4. Conclusions

In this work, we described the application of an RRDE setup to measure rates of the Chlorine Evolution Reaction (CER) in the context of selectivity between CER and the Oxygen Evolution Reaction (OER) in acidic aqueous media. We used a Pt ring to selectively reduce the Cl_2 formed on the disk by fixing the ring potential at 0.95 V vs. RHE in pH 0.88, which gives reliable diffusion-limited CER rates while allowing precise and flexible data acquisition. Using this method, we demonstrated that OER and CER on a glassy carbon supported IrO_x catalyst proceed independently, and that the selectivity towards chlorine evolution (ε_{CER}) rapidly approaches 100% as [Cl^-] increases from 0 to 100 mM. Moreover, our results suggest that on IrO_x, OER is not suppressed or influenced by the presence of Cl^- or by the CER taking place simultaneously on the surface.

Acknowledgements

This research received funding from the Netherlands Organisation for Scientific Research (NWO) in the framework of the fund New Chemical Innovations, project 731.015.204 ELECTROGAS, with financial support of Akzo Nobel Chemical, Shell Global Solutions, Magneto Special Anodes (Evoqua Water Technologies) and Elson Technologies.

Appendix A. Supplementary data

Supplementary data to this article can be found online at https://doi.org/10.1016/j.jelechem.2017.10.058.

References

[1] S. Trasatti, Electrocatalysis: understanding the success of DSA®, Electrochim. Acta 45 (2000) 2377–2385, http://dx.doi.org/10.1016/S0013-4686(00)00338-8.
[2] R.K.B. Karlsson, A. Cornell, Selectivity between oxygen and chlorine evolution in the chlor-alkali and chlorate processes, Chem. Rev. 116 (2016) 2982–3028, http://dx.doi.org/10.1021/acs.chemrev.5b00389.
[3] S. Trasatti, Progress in the understanding of the mechanism of chlorine evolution at oxide electrodes, Electrochim. Acta 32 (1987) 369–382, http://dx.doi.org/10.1016/0013-4686(87)85001-6.
[4] World Chlorine Counsil, Sustainable progress, downloaded from http://www.worldchlorine.org/wp-content/themes/brickthemewp/pdfs/sustainablefuture.pdf on 19-07-2017, 2017. http://www.worldchlorine.org/wp-content/themes/brickthemewp/pdfs/sustainablefuture.pdf, .
[5] U.S. Department of Energy, Advanced chlor-alkali technology (CPS #1797), Ind. Technol. Progr. (2006) 1–2.
[6] S. Anantharaj, S.R. Ede, K. Sakthikumar, K. Karthick, S. Mishra, S. Kundu, Recent trends and perspectives in electrochemical water splitting with an emphasis on sulfide, selenide, and phosphide catalysts of Fe, Co, and Ni: a review, ACS Catal. 6 (2016) 8069–8097, http://dx.doi.org/10.1021/acscatal.6b02479.
[7] D. Banham, S. Ye, Current status and future development of catalyst materials and catalyst layers for proton exchange membrane fuel cells: an industrial perspective, ACS Energy Lett. 2 (2017) 629–638, http://dx.doi.org/10.1021/acsenergylett.6b00644.
[8] M. Shao, Q. Chang, J.-P. Dodelet, R. Chenitz, Recent advances in electrocatalysts for oxygen reduction reaction, Chem. Rev. 116 (2016) 3594–3657, http://dx.doi.org/10.1021/acs.chemrev.5b00462.
[9] M.G. Walter, E.L. Warren, J.R. McKone, S.W. Boettcher, Q. Mi, E. Santori, N.S. Lewis, Solar water splitting cells, Chem. Rev. 110 (2010) 6446–6473, http://dx.doi.org/10.1021/cr1002326.
[10] S. Chen, Y. Zheng, S. Wang, X. Chen, Ti/RuO_2-Sb_2O_5-SnO_2 electrodes for chlorine evolution from seawater, Chem. Eng. J. 172 (2011) 47–51, http://dx.doi.org/10.1016/j.cej.2011.05.059.
[11] P. Duby, The history of progress in dimensionally stable anodes, JOM 45 (1993) 41–43, http://dx.doi.org/10.1007/BF03222350.
[12] G. Chen, Electrochemical technologies in wastewater treatment, Sep. Purif. Technol. 38 (2004) 11–41, http://dx.doi.org/10.1016/j.seppur.2003.10.006.
[13] C.A. Martínez-Huitle, S. Ferro, Electrochemical oxidation of organic pollutants for the wastewater treatment: direct and indirect processes, Chem. Soc. Rev. 35 (2006) 1324–1340, http://dx.doi.org/10.1039/B517632H.
[14] J. Naumczyk, L. Szpyrkowicz, F. Zilio-Grandi, Electrochemical treatment of textile wastewater, Water Sci. Technol. 34 (1996) 17–24, http://dx.doi.org/10.1016/S0273-1223(96)00816-5.
[15] S.H. Lin, C.L. Wu, Electrochemical nitrite and ammonia removal from aqueous solution, J. Environ. Sci. Health. Part A Environ. Sci. Eng. Toxicol. 30 (1995) 1445–1456, http://dx.doi.org/10.1080/10934529509376277.
[16] S. Trasatti, Electrocatalysis in the anodic evolution of oxygen and chlorine, Electrochim. Acta 29 (1984) 1503–1512, http://dx.doi.org/10.1016/0013-4686(84)85004-5.
[17] K.S. Exner, J. Anton, T. Jacob, H. Over, Controlling selectivity in the chlorine evolution reaction over RuO_2-based catalysts, Angew. Chem. Int. Ed. 53 (2014) 11032–11035, http://dx.doi.org/10.1002/anie.201406112.
[18] H.A. Hansen, I.C. Man, F. Studt, F. Abild-Pedersen, T. Bligaard, J. Rossmeisl, Electrochemical chlorine evolution at rutile oxide (110) surfaces, Phys. Chem. Chem. Phys. 12 (2010) 283–290, http://dx.doi.org/10.1039/B917459A.
[19] B.E. Conway, M. Novák, Chloride ion adsorption effects in the recombination-controlled kinetics of anodic chlorine evolution at Pt electrodes, J. Chem. Soc. Faraday Trans. 1 Phys. Chem. Condens. Phases 75 (1979) 2454–2472, http://dx.doi.org/10.1039/F19797502454.
[20] V. Consonni, S. Trasatti, F. Pollak, W.E. O'Grady, Mechanism of chlorine evolution on oxide anodes study of pH effects, J. Electroanal. Chem. 228 (1987) 393–406, http://dx.doi.org/10.1016/0022-0728(87)80119-5.
[21] S. Ferro, A. De Battisti, I. Duo, C. Comninellis, W. Haenni, A. Perret, Chlorine

evolution at highly boron-doped diamond electrodes, J. Electrochem. Soc. 147 (2000) 2614–2619, http://dx.doi.org/10.1149/1.1393578.
[22] S. Ferro, A. De Battisti, Electrocatalysis and chlorine evolution reaction at ruthenium dioxide deposited on conductive diamond, J. Phys. Chem. B 106 (2002) 2249–2254, http://dx.doi.org/10.1021/jp012195i.
[23] S.V. Evdokimov, Mechanism of chlorine evolution-ionization on dimensionally stable anodes, Russ. J. Electrochem. 36 (2000) 227–230, http://dx.doi.org/10.1007/BF02827964.
[24] V.V. Panić, A.B. Dekanski, S.K. Milonjić, R. Atanasoski, B.Ž. Nikolić, The influence of the aging time of RuO_2 and TiO_2 sols on the electrochemical properties and behavior for the chlorine evolution reaction of activated titanium anodes obtained by the sol-gel procedure, Electrochim. Acta 46 (2000) 415–421, http://dx.doi.org/10.1016/S0013-4686(00)00600-9.
[25] M.F. Reznik, D.M. Shub, E.V. Kasatkin, N.V. Kozlova, Anodic oxide-film of the Co—Sn—O composition, Russ. J. Electrochem. 36 (2000) 889–892, http://dx.doi.org/10.1007/BF02757064.
[26] O. Wolter, J. Heitbaum, Differential electrochemical mass spectroscopy (DEMS) - a new method for the study of electrode processes, Berichte Der Bunsengesellschaft Für Phys. Chemie. 88 (1984) 2–6, http://dx.doi.org/10.1002/bbpc.19840880103.
[27] H. Oberacher, F. Pitterl, R. Erb, S. Plattner, Mass spectrometric methods for monitoring redox processes in electrochemical cells, Mass Spectrom. Rev. 34 (2015) 64–92, http://dx.doi.org/10.1002/mas.21409.
[28] Y. Takasu, T. Arikawa, S. Sunohara, K. Yahikozawa, Direct detection of competitively evolving chlorine and oxygen at anodes, J. Electroanal. Chem. 361 (1993) 279–281, http://dx.doi.org/10.1016/0022-0728(93)87067-6.
[29] T. Arikawa, Y. Murakami, Y. Takasu, Simultaneous determination of chlorine and oxygen evolving at RuO_2/Ti and RuO_2–TiO_2/Ti anodes by differential electrochemical mass spectroscopy, J. Appl. Electrochem. 28 (1998) 511–516, http://dx.doi.org/10.1023/A:1003269228566.
[30] K.M. Macounová, M. Makarova, J.S. Jirkovský, J. Franc, P. Krtil, Parallel oxygen and chlorine evolution on $Ru1-xNixO_2-y$ nanostructured electrodes, Electrochim. Acta 53 (2008) 6126–6134, http://dx.doi.org/10.1016/j.electacta.2007.11.014.
[31] V. Petrykin, K.M. Macounová, O. Shlyakhtin, P. Krtil, Tailoring the selectivity for electrocatalytic oxygen evolution on ruthenium oxides by zinc substitution, Angew. Chem. Int. Ed. 49 (2010) 4813–4815, http://dx.doi.org/10.1002/anie.200907128.
[32] K.M. Macounová, N. Simic, E. Ahlberg, P. Krtil, Electrochemical water splitting based on hypochlorite oxidation, J. Am. Chem. Soc. 137 (2015) 1–5, http://dx.doi.org/10.1021/jacs.5b02087.
[33] F. Dionigi, T. Reier, Z. Pawolek, M. Gliech, P. Strasser, Design criteria, operating conditions, and nickel-iron hydroxide catalyst materials for selective seawater electrolysis, ChemSusChem 9 (2016) 962–972, http://dx.doi.org/10.1002/cssc.201501581.
[34] K. Izumiya, E. Akiyama, H. Habazaki, N. Kumagai, a. Kawashima, K. Hashimoto, Anodically deposited manganese oxide and manganese–tungsten oxide electrodes for oxygen evolution from seawater, Electrochim. Acta 43 (1998) 3303–3312, http://dx.doi.org/10.1016/S0013-4686(98)00075-9.
[35] D.F. Abbott, V. Petrykin, M. Okube, Z. Bastl, S. Mukerjee, P. Krtil, Selective chlorine evolution catalysts based on mg-doped nanoparticulate ruthenium dioxide, J. Electrochem. Soc. 162 (2014) H23–H31, http://dx.doi.org/10.1149/2.0541501jes.
[36] T. Le Luu, J. Kim, J. Yoon, Physicochemical properties of RuO_2 and IrO_2 electrodes affecting chlorine evolutions, J. Ind. Eng. Chem. 21 (2015) 400–404, http://dx.doi.org/10.1016/j.jiec.2014.02.052.
[37] C.C.L. McCrory, S. Jung, J.C. Peters, T.F. Jaramillo, Benchmarking heterogeneous electrocatalysts for the oxygen evolution reaction, J. Am. Chem. Soc. 135 (2013) 16977–16987, http://dx.doi.org/10.1021/ja407115p.
[38] J. Scholz, M. Risch, K.A. Stoerzinger, G. Wartner, Y. Shao-Horn, C. Jooss, Supporting information for: rotating ring–disk electrode study of oxygen evolution at a perovskite surface: correlating activity to manganese concentration, J. Phys. Chem. C 120 (2016) 27746–27756, http://dx.doi.org/10.1021/acs.jpcc.6b07654.
[39] I. Spanos, A.A. Auer, S. Neugebauer, X. Deng, H. Tüysüz, R. Schlögl, Standardized benchmarking of water splitting catalysts in a combined electrochemical flow cell/inductively coupled plasma-optical emission spectrometry (ICP-OES) setup, ACS Catal. 7 (2017) 3768–3778, http://dx.doi.org/10.1021/acscatal.7b00632.
[40] N.M. Markovic, H.A. Gasteiger, P.N. Ross, Oxygen reduction on platinum low-index single-crystal surfaces in sulfuric acid solution: rotating ring-Pt(hkl) disk studies, J. Phys. Chem. 99 (1995) 3411–3415, http://dx.doi.org/10.1021/j100011a001.
[41] A.J.J. Jebaraj, N.S. Georgescu, D.A. Scherson, Oxygen and hydrogen peroxide reduction on polycrystalline platinum in acid electrolytes: effects of bromide adsorption, J. Phys. Chem. C 120 (2016) 16090–16099, http://dx.doi.org/10.1021/acs.jpcc.5b12779.
[42] V.R. Stamenkovic, N.M. Markovic, P.N. Ross, Structure-relationships in electrocatalysis: oxygen reduction and hydrogen oxidation reactions on Pt(111) and Pt(100) in solutions containing chloride ions, J. Electroanal. Chem. 500 (2001) 44–51, http://dx.doi.org/10.1016/S0022-0728(00)00352-1.
[43] M. Thomassen, B. Børresen, G. Hagen, R. Tunold, Chlorine reduction on platinum and ruthenium: the effect of oxide coverage, Electrochim. Acta 50 (2005) 1157–1167, http://dx.doi.org/10.1016/j.electacta.2004.08.013.
[44] M. Thomassen, C. Karlsen, B. Børresen, R. Tunold, Kinetic investigation of the chlorine reduction reaction on electrochemically oxidised ruthenium, Electrochim. Acta 51 (2006) 2909–2918, http://dx.doi.org/10.1016/j.electacta.2005.08.024.
[45] S. Vesztergom, M. Ujvári, G.G. Láng, Dual cyclic voltammetry with rotating ring–disk electrodes, Electrochim. Acta 110 (2013) 49–55, http://dx.doi.org/10.1016/j.electacta.2013.01.142.
[46] S. Vesztergom, N. Barankai, N. Kovács, M. Ujvári, H. Siegenthaler, P. Broekmann, G.G. Láng, Electrical cross-talk in four-electrode experiments, J. Solid State Electrochem. 20 (2016) 3165–3177, http://dx.doi.org/10.1007/s10008-016-3294-4.
[47] K.E. Michaux, R.W. Murray, Formation of iridium(IV) oxide (IrOX) films by electroflocculation, Langmuir 29 (2013) 12254–12258, http://dx.doi.org/10.1021/la4025876.
[48] T. Nakagawa, C.A. Beasley, R.W. Murray, Efficient electro-oxidation of water near its reversible potential by a mesoporous IrO_x nanoparticle film, J. Phys. Chem. C 113 (2009) 12958–12961, http://dx.doi.org/10.1021/jp9060076.
[49] Y. Zhao, E.A. Hernandez-Pagan, N.M. Vargas-Barbosa, J.L. Dysart, T.E. Mallouk, A high yield synthesis of ligand-free iridium oxide nanoparticles with high electrocatalytic activity, J. Phys. Chem. Lett. 2 (2011) 402–406, http://dx.doi.org/10.1021/jz200051c.
[50] P. Steegstra, E. Ahlberg, Involvement of nanoparticles in the electrodeposition of hydrous iridium oxide films, Electrochim. Acta 68 (2012) 206–213, http://dx.doi.org/10.1016/j.electacta.2012.02.058.
[51] J. Bennett, Electrodes for generation of hydrogen and oxygen from seawater, Int. J. Hydrog. Energy 5 (1980) 401–408, http://dx.doi.org/10.1016/0360-3199(80)90021-X.
[52] M.T.M. Koper, Thermodynamic theory of multi-electron transfer reactions: implications for electrocatalysis, J. Electroanal. Chem. 660 (2011) 254–260, http://dx.doi.org/10.1016/j.jelechem.2010.10.004.
[53] H.Y. Song, N.B. Kondrikov, V.G. Kuryavy, Y.H. Kim, Preparation and characterization of manganese dioxide electrodes for highly selective oxygen evolution during diluted chloride solution electrolysis, Young 13 (2007) 545–551.
[54] A. Cornell, B. Håkansson, G. Lindbergh, Ruthenium-based dimensionally stable anode in chlorate electrolysis, J. Electrochem. Soc. 150 (2003) D6, http://dx.doi.org/10.1149/1.1522386.
[55] J. Wu, Kinetics of the reduction of hypochlorite ion, J. Electrochem. Soc. 134 (1987) 1462, http://dx.doi.org/10.1149/1.2100690.
[56] G. Lindbergh, D. Simonsson, The effect of chromate addition on cathodic reduction of hypochlorite in hydroxide and chlorate solutions, J. Electrochem. Soc. 137 (1990) 3094, http://dx.doi.org/10.1149/1.2086165.
[57] N. Danilovic, R. Subbaraman, K.-C. Chang, S.H. Chang, Y. Kang, J. Snyder, A.P. Paulikas, D. Strmcnik, Y.T. Kim, D.J. Myers, V.R. Stamenkovic, N.M. Markovic, Supporting information for activity-stability trends for the oxygen evolution reaction on monometallic oxides in acidic environments, J. Phys. Chem. Lett. 5 (2014) 2474–2478, http://dx.doi.org/10.1021/jz501061n.
[58] Y. Zhao, N.M. Vargas-Barbosa, E.A. Hernandez-Pagan, T.E. Mallouk, Anodic deposition of colloidal iridium oxide thin films from hexahydroxyiridate(IV) solutions, Small 7 (2011) 2087–2093, http://dx.doi.org/10.1002/smll.201100485.
[59] I.V. Kadija, B.Ž. Nikolić, A.R. Despić, Mass transfer during gas evolution on the rotating double-ring electrode, J. Electroanal. Chem. Interfacial Electrochem. 57 (1974) 35–52, http://dx.doi.org/10.1016/S0022-0728(74)80005-7.
[60] V.V. Losev, N.Y. Buné, L.E. Chuvaeva, Specific features of the kinetics of gas-evolving reactions on highly active electrodes, Electrochim. Acta 34 (1989) 929–942, http://dx.doi.org/10.1016/0013-4686(89)80017-9.
[61] L.J.J. Janssen, Mass transfer at rotating ring-cone electrodes, J. Appl. Electrochem. 22 (1992) 1091–1094, http://dx.doi.org/10.1007/BF01029591.
[62] J. Suntivich, K.J. May, H.A. Gasteiger, J.B. Goodenough, Y. Shao-Horn, A perovskite oxide optimized for oxygen evolution catalysis from molecular orbital principles, Science 334 (2011) 1383–1385, http://dx.doi.org/10.1126/science.1212858 (80-.).
[63] Q. Gao, C. Ranjan, Z. Pavlovic, R. Blume, R. Schlögl, Enhancement of stability and activity of MnO_x/Au electrocatalysts for oxygen evolution through adequate electrolyte composition, ACS Catal. 5 (2015) 7265–7275, http://dx.doi.org/10.1021/acscatal.5b01632.
[64] M. Alkan, M. Oktay, M.M. Kocakerim, M. Çopur, Solubility of chlorine in aqueous hydrochloric acid solutions, J. Hazard. Mater. 119 (2005) 13–18, http://dx.doi.org/10.1016/j.jhazmat.2004.11.001.
[65] T.J. Schmidt, U.A. Paulus, H.A. Gasteiger, R.J. Behm, The oxygen reduction reaction on a Pt/carbon fuel cell catalyst in the presence of chloride anions, J. Electroanal. Chem. 508 (2001) 41–47, http://dx.doi.org/10.1016/S0022-0728(01)00499-5.
[66] B.E. Conway, M. Novák, Electrocatalytic effect of the oxide film at Pt anodes on Cl· recombination kinetics in chlorine evolution, J. Electroanal. Chem. Interfacial Electrochem. 99 (1979) 133–156, http://dx.doi.org/10.1016/S0022-0728(79)80243-0.
[67] B.E. Conway, G. Ping, Evaluation of Cl· adsorption in anodic Cl_2 evolution at Pt by means of impedance and potential-relaxation experiments. Influence of the state of surface oxidation of the Pt, J. Chem. Soc. Faraday Trans. 87 (1991) 2705, http://dx.doi.org/10.1039/ft9918702705.
[68] K.S. Exner, J. Anton, T. Jacob, H. Over, Chlorine evolution reaction on RuO2(110): Ab initio atomistic thermodynamics study - Pourbaix diagrams, Electrochim. Acta 120 (2014) 460–466, http://dx.doi.org/10.1016/j.electacta.2013.11.027.
[69] K.S. Exner, J. Anton, T. Jacob, H. Over, Full kinetics from first principles of the chlorine evolution reaction over a RuO_2 (110) model electrode, Angew. Chem. Int. Ed. 55 (2016) 7501–7504, http://dx.doi.org/10.1002/anie.201511804.
[70] V. Petrykin, K.M. Macounová, M. Okube, S. Mukerjee, P. Krtil, Local structure of Co

doped RuO_2 nanocrystalline electrocatalytic materials for chlorine and oxygen evolution, Catal. Today 202 (2013) 63–69, http://dx.doi.org/10.1016/j.cattod.2012.03.075.

[71] E. Kuznetsova, V. Petrykin, S. Sunde, P. Krtil, Selectivity of nanocrystalline IrO_2-based catalysts in parallel chlorine and oxygen evolution, Electrocatalysis 6 (2015) 198–210, http://dx.doi.org/10.1007/s12678-014-0233-y.

[72] M.G. Samant, K. Kunimatsu, H. Seki, M.R. Philpott, In situ FTIR study of the adsorption geometry of bisulfate accepted ions on a platinum electrode, J. Electroanal. Chem. 280 (1990) 391–401, http://dx.doi.org/10.1016/0022-0728(90)87012-9.

[73] C. Spöri, J.T.H. Kwan, A. Bonakdarpour, D.P. Wilkinson, P. Strasser, The stability challenges of oxygen evolving catalysts: towards a common fundamental understanding and mitigation of catalyst degradation, Angew. Chem. Int. Ed. 56 (2017) 5994–6021, http://dx.doi.org/10.1002/anie.201608601.

[74] A.A. Topalov, I. Katsounaros, M. Auinger, S. Cherevko, J.C. Meier, S.O. Klemm, K.J.J. Mayrhofer, Dissolution of platinum: limits for the deployment of electrochemical energy conversion? Angew. Chem. Int. Ed. 51 (2012) 12613–12615, http://dx.doi.org/10.1002/anie.201207256.